Available online at www.sciencedirect.com

ScienceDirect

Advances in Space Research 55 (2015) 1234–1240

ADVANCES IN SPACE RESEARCH (a COSPAR publication)

www.elsevier.com/locate/asr

Effect of terrestrial radiation on brightness temperature at lunar nearside: Based on theoretical calculation and data analysis

Guangfei Wei [a,b,*], Xiongyao Li [a], Shijie Wang [a]

[a] Lunar and Planetary Science Research Center, Institute of Geochemistry Chinese Academy of Sciences, Guiyang 550002, China
[b] University of Chinese Academy of Sciences, Beijing 100049, China

Received 13 May 2014; received in revised form 12 November 2014; accepted 17 November 2014
Available online 24 November 2014

Abstract

Terrestrial radiation is another possible source of heat in lunar thermal environment at its nearside besides the solar illumination. On the basis of Clouds and the Earth's Radiant Energy System (CERES) data products, the effect of terrestrial radiation on the brightness temperature (TB_e) of the lunar nearside has been theoretically calculated. It shows that the mafic lunar mare with high TB_e is more sensitive to terrestrial radiation than the feldspathic highland with low TB_e value. According to the synchronous rotation of the Moon, we extract TB_e on lunar nearside using the microwave radiometer data from the first Chinese lunar probe Chang'E-1 (CE-1). Consistently, the average TB_e at Mare Serenitatis is about 1.2 K while the highland around the Geber crater (19.4°S, 13.9°E) is relatively small at ~0.4 K. Our results indicate that there is no significant effect of terrestrial radiation on TB_e at the lunar nearside. However, to extract TB_e accurately, effects of heat flow, rock abundance and subsurface rock fragments which are more significant should be considered in the future work.

Keywords: Chang'E; Brightness temperature; Terrestrial radiation; Moon

1. Introduction

Terrestrial radiation including short and longwave radiations are expected to be additional sources of heat in lunar surface thermal environment at its nearside (Woolf et al., 2002; Goode and Dziembowski, 2003; Huang, 2008). The sustained ground-based observations of earthshine (reflected sunlight) have been made from Big Bear Solar Observatory since late 1998, and they showed that the Earth's albedo decreased during 1985–2000 (Qiu et al., 2003; Pall et al., 2005). Based on high quality of satellite measurements such as Earth Radiation Budget Experiment (ERBE) and, Clouds and the Earth's Radiant Energy System (CERES), it has been reported that the Earth's outgoing radiation did not remain constant throughout a year (Wielicki et al., 1996; Priestley et al., 2010). Therefore, it can be inferred that the Earth's radiation reaching the Moon would also vary, and it might play a part in the lunar surface thermal environment, especially during nighttime.

Previous work indicated that terrestrial radiation reaching the Moon is larger than lunar heat flow measured by Apollo15 and 17 missions (Langseth et al., 1976; Huang, 2008). Therefore, it may have a relatively larger impact on the radiation characteristics of the lunar surface such as evaporating the putative ice deposits on the permanently shadowed lunar polar craters (Head, 2006). The regolith temperature at nearside, on the contrary, would amplify terrestrial radiation signal (Huang, 2008). To characterize

* Corresponding author at: Lunar and Planetary Science Research Center, Institute of Geochemistry Chinese Academy of Sciences, Guiyang 550002, China.
E-mail addresses: gfwei0554@gmail.com (G. Wei), lixiongyao@vip.skleg.cn (X. Li).

http://dx.doi.org/10.1016/j.asr.2014.11.011
0273-1177/

regolith thermal behavior affected by terrestrial radiation, here, we assumed that only the top dust layer (2 cm thick) was affected by terrestrial radiation because of its high insulation that restrains the downward heat flux.

China had launched a lunar probe Chang'E-1 (CE-1) on October 24, 2007 successfully. The scientific objective of microwave radiometer (MRM) aboard CE-1 was to explore lunar surface thermal radiation characteristics from 200 km orbit by monitoring four bands, 3.0, 7.8, 19.35, and 37 GHz. It provided radiometric resolution of 0.5 K and a spatial resolution (56 km for the first band and 30 km for other bands), better than any ground-based microwave observation (Zheng et al., 2012). During its life time of more than one year, large amount of brightness temperature (TB) data covering the Moon globally several times were obtained. Locked in synchronous rotation, only the nearside of the Moon that faces Earth receives terrestrial radiation constantly. That means the TB data at nearside includes terrestrial radiation information while the farside is not. Therefore, the TB_e data affected by terrestrial radiation at lunar nearside can be extracted from MRM data after the influences of $(FeO + TiO_2)$ and roughness had been removed effectively. As higher frequencies penetrate shallower depths, the TB_e at 37 GHz, that represents the top dust layer only will be considered in this study.

To start with, a theoretical model to estimate TB_e over the nearside has been formulated which is followed by a method to extract TB_e from CE-1's MRM data. Finally the results from both the model and measurements are presented and discussed.

2. Theoretical analysis

2.1. Theoretical model

The "earth phase" is synchronous and complementary to lunar phase due to the Sun–Earth–Moon orbital motion. During the New Moon, the terrestrial radiation has relatively greater impact on lunar nearside because the Earth reflects the solar irradiation from its bright side only. The radiation from the Earth includes shortwave radiation (E_{sw}) reflected from total solar irradiance (TSI) and outgoing longwave radiation (E_{lw}) which corresponds to thermal radiation. Assuming the outward terrestrial radiation E ($E = E_{sw} + E_{lw}$, $W\,m^{-2}$) is isotropic in deep space, the "Total Earth Irradiance" TEI at the distance of the Moon is estimated by Huang (2008) as following

$$TEI = \left(\frac{R_e}{R_{em}}\right)^2 \times E \tag{1}$$

where R_e, R_{em} are Earth radius and Earth–Moon distance, respectively.

In order to estimate the lunar surface temperature responding to TEI, we further assume that the surface of the Moon is a gray-body to the radiation it actually receives during nighttime. On the basis of Stefan–Boltzmann law, the surface temperature for a given site on the nearside of the Moon could be expressed as (Huang, 2008)

$$T_m = \left(\frac{1-r}{\sigma} \times TEI\right)^{1/4} \tag{2}$$

where T_m is the lunar surface temperature affected by TEI in units of Kelvin, σ is Stefan–Boltzmann constant (5.67×10^{-8}), and r is lunar surface reflectivity. Ground based photographic data indicated that the reflectivity of the lunar surface layer was about 0.090–0.228 with an average of 0.125 (Wildey, 1977). Racca also obtained the total solar albedo of lunar surface about 0.127 by regression analysis of disk-integrated measurements (Racca, 1995). In this study, we take this parameter as 0.127 to estimate T_m.

However, in reality, there would be significant downward heat conduction due to the vertical thermal gradient set up between the region that receives the terrestrial radiation and the lunar interior. Unfortunately, there is less knowledge of thermal properties of dust layer in a global scale, thus, it becomes difficult to obtain the temperature profile by employing the heat conduction equation. As an approximation, an isothermal dust layer was assumed to calculate TB_e over the lunar nearside by radiative transfer theory. According to the strong fluctuation theory, TB_e based on the emissions from the dust layer at zero-order polarization and 0° observation angle of CE-1 MRM can be written as (Tsang et al., 1985; Jin, 1993)

$$TB_e = \frac{k_0 \varepsilon''}{2\varepsilon_0 k_d''} |X_{0d}|^2 \left[1 - \exp\left(-2k_d'' d\right)\right] \cdot \left[1 + |R_{ds}|^2 \exp\left(-2k_d'' d\right)\right] \cdot T_m \tag{3}$$

where ε_0 is relative dielectric constant of vacuum, ε'' is imaginary part of dielectric constant of dust layer. k_0 and k_d'' are wave number of free space and dust layer, respectively. R_{ds} and X_{0d} are respectively the reflection coefficient and transmission coefficient between the dust–soil layer and vacuum–dust layer interfaces, and d is the thickness of dust layer.

Laboratory measurement of returned samples shows that the dielectric constant of regolith, $\varepsilon = \varepsilon' + i\varepsilon''$, is given by the bulk density ρ and $(FeO + TiO_2)$ content S as (Heiken et al., 1991)

$$\varepsilon' = 1.919^{\rho} \tag{4}$$

$$\tan\delta = 10^{0.038S + 0.312\rho - 3.26} \tag{5}$$

where $\tan\delta = \varepsilon''/\varepsilon'$ is the dielectric loss of regolith.

2.2. Numerical calculation

The basic step to understand the terrestrial radiation effect on lunar surface thermal radiation characteristics is to quantify the variations of earthshine and thermal radiation reaching the Moon. First of their kinds satellites used to monitor TSI started in 1978 by the National Oceanic

and Atmospheric Administration's Nimbus 7 Earth Radiation Budget Experiment. The ERBE became the first of NASA's missions to provide radiant flux information at the top of atmosphere since 1984 (Smith et al., 2004; Huang, 2008). Up til now, CERES experiment is one of the highest priority scientific satellite instruments and it opens up a new era in radiation–climate observations by providing more accurate and stable products than the previous ERBE (Priestley et al., 2010). CERES products include both solar-reflected and Earth-emitted radiations from both, the top of the atmosphere and the Earth's surface. In this study we selected CERES global monthly mean data (http://ceres.larc.nasa.gov/orderdata.php) corresponding to the time span of CE-1 mission between 11/2007 and 07/2008. On the basis of Eqs. (1) and (2), T_m at the center of nearside was calculated during the New Moon phase in each month (Fig. 1). Obviously, terrestrial radiation decreases substantially from winter (11/2007) to summer (07/2008) while the Moon gets closer to Earth during this period. As a result, T_m increases gradually before reaching the peak. It can be concluded that R_{em} has more effect on the lunar surface thermal environment. In order to obtain TB_e at nearside in a global scale and compare it with CE-1's MRM data products, we chose average E and R_{em} to calculate T_m as described in the following paragraph.

To calculate TB_e by Eq. (3), we first have to get the regolith dielectric constant on the basis of Eqs. (4) and (5). Widely used algorithm for retrieving the content of $(FeO + TiO_2)$ from Clementine multispectral data was derived by Lucey et al. (1998, 2000). It was further evolved by Gillis et al. (2003, 2004) and more reliable results were obtained. In this study, we apply the same algorithms from Gillis et al. (2003, 2004) to retrieve the content of $(FeO + TiO_2)$ at lunar nearside based on Clementine UVVIS data (http://www.lpi.usra.edu/lunar/tools/clementine). Combining with Eqs. (1)–(3), TB_e at lunar nearside were calculated and mapped by orthographic projection in Fig. 2. Apparently, TB_e in lunar mare is relatively higher than that in highland. Some patches located in the northwest of Mare Tranquillitatis can achieve the maximum value of about 1.6 K. It suggests that lunar mare regions are more sensitive to terrestrial radiation than highland. This might be caused by different mineral constituents in the regolith like for instance: more mafic silicate in mare region and feldspathic silicate in highland.

3. Chang'E-1 data analysis

3.1. Methodology

Since the Moon is locked in synchronous rotation with the Earth, TB obtained by CE-1 MRM at nearside includes terrestrial radiation information while the farside does not. Therefore, the TB_e at nearside can be extracted from CE-1's MRM data after the effects of topographic relief and $(FeO + TiO_2)$ have been duly accounted for. It is worth noting that the substructure of lunar regolith within the penetration depth of 37 GHz (~0.5 m) in the study areas between nearside and farside are assumed to be homogenous after a long-term space weathering. Moreover, the deviation of heat flows between the two sides are neglected too.

As shown in Fig. 2, lunar mare is more sensitive to terrestrial radiation, thus, the two candidate areas of Mare Moscoviense (located at farside) and Mare Serenitatis (located at nearside, marked by A) located in the same latitude range were selected. For the nadir-viewing of microwave radiometer, surface roughness effects are not expected to be significant, and the lunar surface could be

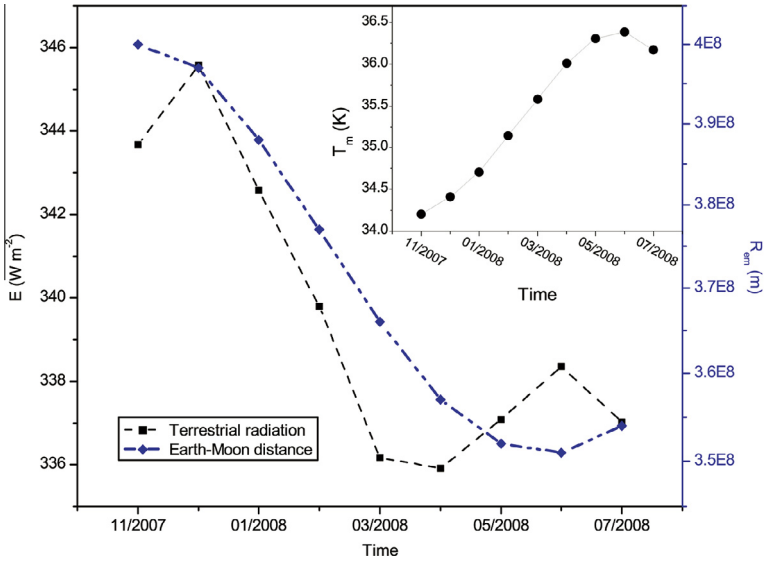

Fig. 1. Variations of terrestrial radiation (E) and Earth–Moon distance (R_{em}) during the New Moon from 11/2007 to 07/2008. The upper right of this panel shows surface temperature (T_m) at center disk affected by terrestrial radiation during this period.

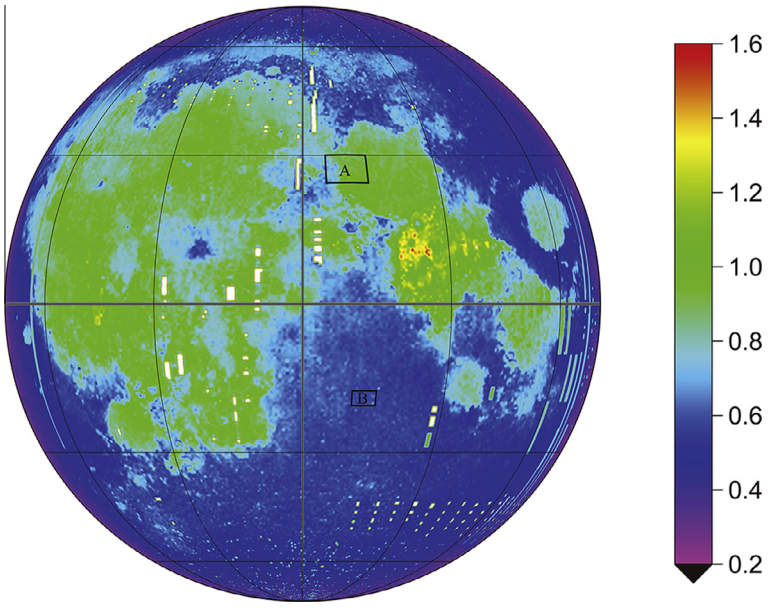

Fig. 2. Effect of terrestrial radiation on TB at lunar nearside during the phase of New Moon at orthographic projection. The average TEI (0.1 W m^{-2}) at center disk is derived from CERES data which presented in Fig. 1. The bulk density of the dust layer, $\rho_d = 1.3$ g cm^{-3}. Note that the fictitious graticule is 30° × 30°. The black boxes marked by A and B are study areas which will be analyzed by CE-1's MRM data latter.

well modeled as a flat surface under the spatial resolution of CE-1's MRM observation, more so for the flat ground in mare regions (Keihm, 1984; Jin and Fa, 2011).

As expressed in Eq. (5), more content of ($FeO + TiO_2$) can lead to higher dielectric loss, and the TB obtained by MRM is expected to be higher (Feng et al., 2010). For more sensitive lunar mare, even a small difference of ($FeO + TiO_2$) between the two study areas might cause TB_e changes. Fig. 3 shows the mosaic of ($FeO + TiO_2$) content at the two study areas. Apparently, ($FeO + TiO_2$) in the study areas are not evenly distributed at high spatial resolution (100 m/pix).

Although, the content of ($FeO + TiO_2$) at highland is very low which approximates to 5% of global mean (Lucey et al., 1998), cratered surface at highland can make local solar illumination rather complex. Various roughness parameters of root mean square (σ) and auto correlation (l), for example, can account for the Moon's topographic features (Shepard et al., 2001; Gupta and Jangid, 2011). The numerical simulation indicated the TB of the lunar surface will increase with the roughness at the observation angle of 0° (He et al., 2013). Here, we take into account σ to characterize surface roughness and in addition a maximum deviation about 2% was considered between nearside and farside areas for the major elements (Si, Ca, Mg, Fe, Ti, Al. The candidate area marked by B in Fig. 2 is presented in Fig. 4.

For the long night on the Moon, TB is also dependent on lunar local time due to the fluctuation of lunar regolith temperature (Jones et al., 1975; Li et al., 2010). That means the TB detected by CE-1 MRM on lunar surface would decrease after sunset and increase again after sunrise (Chan et al., 2010; Zheng et al., 2012). Due to the circular polar track of CE-1's MRM, the TB of the lunar surface

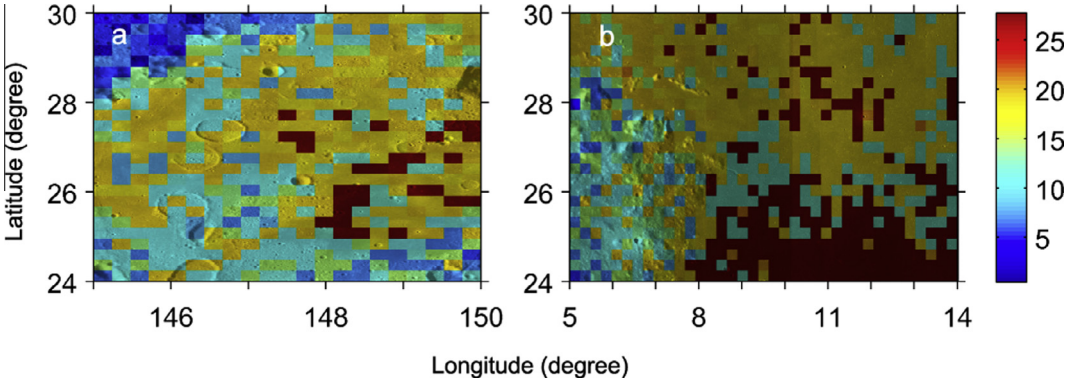

Fig. 3. Mosaic of ($FeO + TiO_2$) content (percentage) in the study areas of Mare Moscoviense (a) and Mare Serenitatis (b). The base maps are acquired from Lunar Reconnaissance Orbiter Wide Angle Camera Mosaic data at a resolution of 100 m/pix.

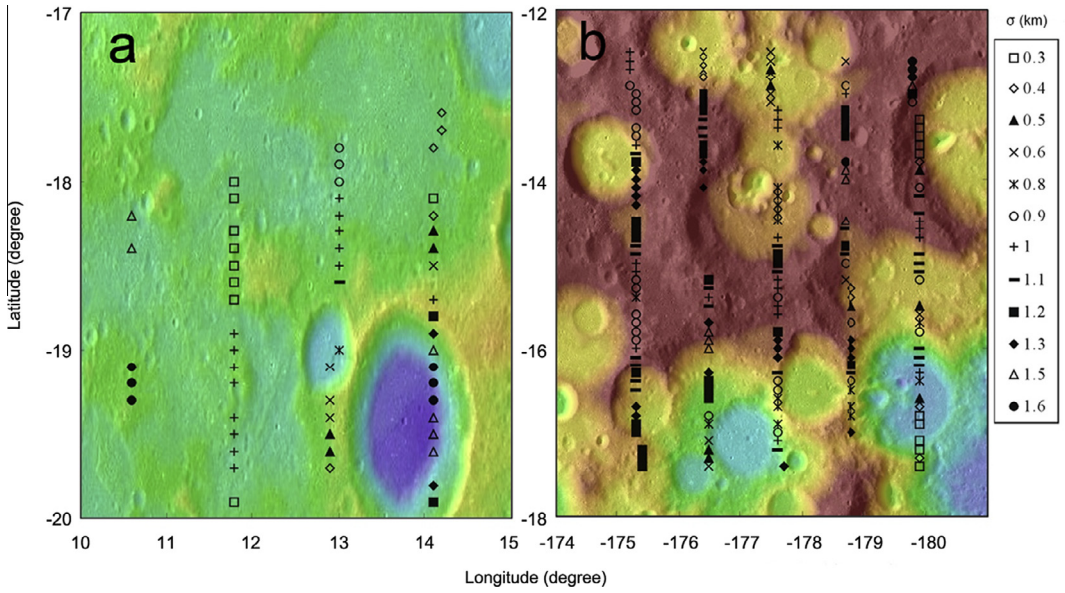

Fig. 4. Distributions of σ at the study area B (around the Geber crater, −19.4°, 13.9°) on the lunar nearside (a) and farside (b). Both of the attached base maps are false color topographic maps drawn from LRO/LOLA data (http://ode.rsl.wustl.edu/moon/indexDatasets.aspx). The roughness parameter σ was calculated on the basis of Clementine topographic data.

could be measured at different lunar local times. The measured TB therefore has both the effects viz., the local time variation in addition to the terrestrial radiation effect. Therefore, before comparing the study areas some sort of a temporal normalization of different study areas in the time domain has to be carried out.

To project the nighttime TB data to their midnight (local time 0) value for any point on the lunar surface, we normalized the observed TB data to midnight value at the study areas A and B based on Eqs. (6) and (7) as had been done in the work of Zheng et al. (2012).

$$TB_{h(model)} = B + \sum_{i=1}^{7}\left(B_i \times h^i\right) \tag{6}$$

$$TB_{midnight(normalized)} = TB_{h(measured)} \times TB_{midnight(model)}/TB_{h(model)} \tag{7}$$

where $TB_{h(model)}$ is the model value given by Eq. (6) at the local time h (in the range of 0–24), $B, B_1, \ldots, B_7$ are constants of this degree-seven polynomial fitting scheme, $TB_{h(measured)}$ is the TB data measured by CE-1 MRM at local time h, $TB_{midnight(model)}$ is the fitted model TB value at midnight, and $TB_{midnight(normalized)}$ is the normalized value of measured TB at midnight.

3.2. Results and discussion

On the basis of Eqs. (6) and (7), the filtered MRM data covering the study areas (A and B) were normalized to midnight time values ($TB_{midnight(normalized)}$). Fig. 5 shows TB_e versus different content of $(FeO + TiO_2)$ in A. Consistently, the average TB_e (~1.3 K) extracted from temporally normalized data is a little greater than that has been estimated

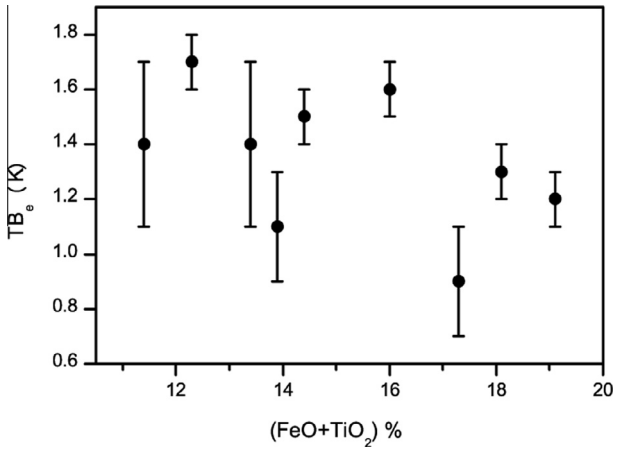

Fig. 5. Effect of terrestrial radiation on TB versus the content of $(FeO + TiO_2)$ at the study area A. The uncertainty bars represent the standard deviation from the mean.

by numerical calculation (~1.0 K), but limited to the resolution of 0.5 K. It is worth noting that the TB_e is very sensitive to the content of $(FeO + TiO_2)$ though the functional relation is not obvious here.

For the cratered highland, Fig. 6 (lower panel) shows similar trend of TB versus σ. It suggests similar effects on TB at the same roughness on both sides. Therefore, it is feasible to extract TB_e at the study area B from these data. As presented in the upper panel of Fig. 6, TB_e varies from 0.2 to 0.6 K at different surface roughness. Although TB_e at this highland area is really inappreciable compared with TB emitted from the regolith layer (lower panel), the average one (~0.4 K) still approximates to our numerical result (~0.5 K) which confirms the data analysis.

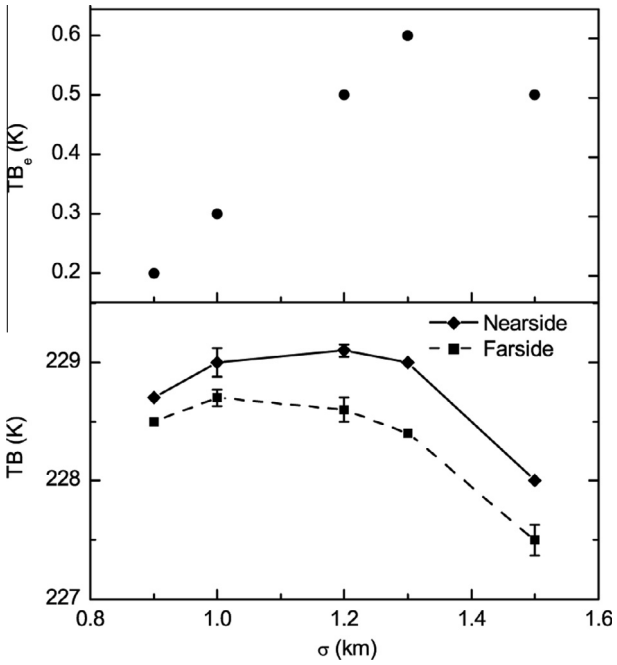

Fig. 6. TB/TB$_e$ versus surface roughness. The lower panel shows the temporal normalized TB at both sides corresponding to different σ in Fig. 4. The error bars indicate the standard deviation of normalized results. The upper panel shows the distributions of TB$_e$ at different roughness.

Similar to the content of ($FeO + TiO_2$), heat flow might be another important parameter that could affect TB$_e$ besides terrestrial radiation in lunar night. To extract TB$_e$ from MRM data accurately, we have to take into account the heat flow effect. Ground based observation indicated that lunar heat flow ranged from 0.01 W m^{-2} to 0.033 W m^{-2} (Troitskiy and Tikhonova, 1971). Revised heat flow values at Hadley Rille (Apollo 15 landing area) and Taurus–Littrow (Apollo 17 landing area) were 0.021 W m^{-2} and 0.016 W m^{-2}, respectively (Langseth et al., 1976). Based on a model of the crustal abundance of U, Th, K, topography and inferred crustal thickness, the average global heat flow was estimated to be 0.018 W m^{-2} which was about 19% to the maximum TEI reaching the Moon (Langseth et al., 1976; Huang, 2008). Therefore, heat flow might cause TB difference between nearside and farside, especially at lunar mare which is rich in radioactive elements.

Here, we aim to compare the abundance of radioactive elements in the study areas as shown in Fig. 3. Table 1 shows the average content of radioactive elements (U, Th, K) in Mare Moscoviense and Mare Serenitatis limited in the range of Fig. 3, and they are retrieved from Lunar Prospector Reduced Spectrometer source data provided by the PDS Geosciences Node at 2 pix/deg (http://www.mapaplanet.org/explorer/moon.html). Obviously, there are more radioactive elements in Mare Serenitatis which can produce greater heat flow that will have a substantial effect on TB$_e$. Moreover, rock abundance in the craters and, subsurface rock fragments also affect surface thermal radiation, especially at cratered highland areas (Alekseev et al., 1968; Keihm, 1984; Bandfield et al., 2011; He et al., 2013). To quantify these effects, more efforts will be performed in the future work.

Table 1
Average content of radioactive elements (ppm) in Mare Moscoviense and Mare Serenitatis limited in the range of Fig. 3.

Study area	U	Th	K
Mare Moscoviense	0.5	1.8	413
Mare Serenitatis	1.5	4.2	1739

4. Conclusion

Terrestrial radiation, including shortwave and longwave radiations is another heat source in lunar surface thermal environment at nearside besides the solar illumination. On the basis of Clouds and the Earth's Radiant Energy System data products, the effect of terrestrial radiation on TB at nearside was calculated theoretically during the New Moon. It indicates TB$_e$ at mafic mare is more sensitive to terrestrial radiation than the feldspathic highland. Because lunar nearside always faces Earth, i.e. only nearside receives Earth radiation while the farside does not, we have extracted TB$_e$ from CE-1 MRM data (37 GHz) at the study areas A (lunar mare) and B (lunar highland). Our results show that they are consistent with numerical calculations: the average of TB$_e$ at A is about 1.3 K while it is about 0.4 K at B. These results show that there is no significant effect of terrestrial radiation on TB at lunar nearside.However, to extract TB$_e$ accurately from MRM data, the effects of heat flow, rock abundance, subsurface rock fragments on TB should be properly accounted for.

Acknowledgments

We would like to thank Prof. Wenzhe Fa (Peking University) and two anonymous reviewers for their constructive comments in this study. This study was supported by National Natural Science Foundation of China (Grant Nos. 41373067, 41403057 and 41403059) and the West Light Foundation of The Chinese Academy of Sciences.

References

Alekseev, V.A., Aleshina, T.N., Krotikov, V.D., Troitskii, V.S., 1968. The roughness of the moon's surface layer as it affects the lunar emissivity and radio-brightness distribution. Sov. Astron. 11 (5), 1070–1074.

Bandfield, J.L., Ghent, R.R., Vasavada, A.R., Paige, D.A., Lawrence, S.J., Robinson, M.S., 2011. Lunar surface rock abundance and regolith fines temperatures derived from lro diviner radiometer data. J. Geophys. Res. 116 (E12), E00H02.

Chan, K.L., Tsang, K.T., Kong, B., Zheng, Y.-C., 2010. Lunar regolith thermal behavior revealed by Chang'E-1 microwave brightness temperature data. Earth Planet. Sci. Lett. 295 (1), 287–291.

Feng, J., Zou, Y., Bian, W., Zheng, Y., Li, C., 2010. Review on physical models of lunar brightness temperature. Chin. J. Geochem. 29 (2), 204–211.

Gillis, J.J., Jolliff, B.L., Elphic, R.C., 2003. A revised algorithm for calculating TiO2 from clementine uvvis data: a synthesis of rock, soil, and remotely sensed TiO2 concentrations. J. Geophys. Res. 108 (E2), 5009.

Gillis, J.J., Jolliff, B.L., Korotev, R.L., 2004. Lunar surface geochemistry: global concentrations of th, k, and feo as derived from lunar prospector and clementine data. Geochim. Cosmochim. Acta 68 (18), 3791–3805.

Goode, P.R., Dziembowski, W.A., 2003. Sunshine, earthshine and climate change I. Origin of, and limits on solar variability. J. Korean Astron. Soc. 36 (D22), 75–81.

Gupta, V., Jangid, R., 2011. Microwave response of rough surfaces with auto-correlation functions, rms heights and correlation lengths using active remote sensing. Indian J. Radio Space Phys. 40 (3), 137–146.

Head, J.N., 2006. Earthshine at the lunar poles and volatile stability. In: Proc. Lunar Planet. Sci. Conf. 37th 1886.

He, L., Lang, L., Li, Q., Zheng, W., 2013. Effect of surface roughness on microwave brightness temperature from lunar surface: numerical analysis with a hybrid method. Adv. Space Res. 51 (1), 179–187.

Heiken, G.H., Vaniman, D.T., French, B.M., 1991. Lunar Sourcebook – A User's Guide to the Moon. Cambridge University Press, London.

Huang, S., 2008. Surface temperatures at the nearside of the moon as a record of the radiation budget of earths climate system. Adv. Space Res. 41 (11), 1853–1860.

Jin, Y., 1993. Electromagnetic Scattering Modelling for Quantitative Remote Sensing. World Scientific.

Jin, Y., Fa, W., 2011. The modeling analysis of microwave emission from stratified media of non-uniform lunar cratered terrain surface for Chinese Chang-E 1 observation. Chin. Sci. Bull. 56 (11), 1165–1171.

Jones, W.P., Watkins, J.R., Calvert, T.A., 1975. Temperatures and thermophysical properties of the lunar outermost layer. Earth Moon Planets 13 (975), 475–494.

Keihm, S.J., 1984. Interpretation of the lunar microwave brightness temperature spectrum: feasibility of orbital heat flow mapping. Icarus 60 (3), 568–589.

Langseth, M.G., Keihm, S.J., Peters, K., 1976. Revised lunar heat-flow values. In: Proc Lunar Planet. Sci. Conf. 7th, vol. 7, pp. 3143–3171.

Li, Y., Wang, Z., Jiang, J., 2010. Simulations on the influence of lunar surface temperature profiles on ce-1 lunar microwave sounder brightness temperature. Sci. China Earth Sci. 53 (9), 1379–1391.

Lucey, P.G., Blewett, D.T., Hawke, B.R., 1998. Mapping the FeO and TiO2 content of the lunar surface with multispectral imagery. J. Geophys. Res. 103 (E2), 3679–3699.

Lucey, P.G., Blewett, D.T., Hawke, B.R., 2000. Lunar iron and titanium abundance algorithms based on final processing of clementine ultraviolet-visible images. J. Geophys. Res. 105 (E8), 20297–20305.

Pall, E., Montas-Rodriguez, P., Goode, P.R., Koonin, S.E., Wild, M., Casadio, S., 2005. A multi-data comparison of shortwave climate forcing changes. Geophys. Res. Lett. 32 (21).

Priestley, K.J., Smith, G.L., Thomas, S., Cooper, D., Lee, R.B., Walikainen, D., Hess, P., Szewczyk, Z.P., Wilson, R., 2010. Radiometric performance of the ceres earth radiation budget climate record sensors on the eos aqua and terra spacecraft through April 2007. J. Atmos. Oceanic Technol. 28 (1), 3–21.

Qiu, J., Goode, P.R., Pall, E., Yurchyshyn, V., 2003. Earthshine and the earth's albedo: 1. Earthshine observations and measurements of the lunar phase function for accurate measurements of the earth's bond albedo. J. Geophys. Res. 108 (D22).

Racca, G.D., 1995. Moon surface thermal characteristics for moon orbiting spacecraft thermal analysis. Planet. Space Sci. 633 (6), 835–842.

Shepard, M.K., Campbell, B.A., Bulmer, M.H., Farr, T.G., Gaddis, L.R., Plaut, J.J., 2001. The roughness of natural terrain: a planetary and remote sensing perspective. J. Geophys. Res. 106 (E12), 32777–32795.

Smith, G.L., Wielicki, B.A., Barkstrom, B.R., Lee, R.B., Priestley, K.J., Charlock, T.P., Minnis, P., Kratz, D.P., Loeb, N., Young, D.F., 2004. Clouds and earth radiant energy system: an overview. Adv. Space Res. 33 (7), 1125–1131.

Troitskiy, V., Tikhonova, T., 1971. Thermal radiation from the moon and the physical properties of its upper mantle. Nasa technical translation.

Tsang, L., Kong, J., Robert, T.S., 1985. Theory of Microwave Remote Sensing. John Wiley and Sons, Incorporated.

Wielicki, B.A., Barkstrom, B.R., Harrison, E.F., Lee, R.B., Louis Smith, G., Cooper, J.E., 1996. Clouds and the earth's radiant energy system (ceres): an earth observing system experiment. Bull. Am. Meteorol. Soc. 77 (5), 853–868.

Wildey, R.L., 1977. A digital file of the lunar normal albedo. Earth Moon Planets 16, 231–277.

Woolf, N.J., Smith, P.S., Traub, W.A., Jucks, K.W., 2002. The spectrum of earthshine a pale blue dot observed from the ground. Astrophys. J. 574, 430–433.

Zheng, Y., Tsang, K., Chan, K., Zou, Y., Zhang, F., Ouyang, Z., 2012. First microwave map of the moon with change-1 data: the role of local time in global imaging. Icarus 219 (1), 194–210.